

Comparison of hydrographic and altimeter based estimates of sea level height variability in the Atlantic Ocean

Dennis A. Mayer, Molly O. Baringer* and Gustavo J. Goni

National Oceanic and Atmospheric Administration,
Atlantic Oceanographic and Meteorological Laboratory,
4301 Rickenbacker Causeway, Miami, Florida, 33149

Our ability to understand the means by which mass and heat are exchanged between the tropics and subtropics is seriously compromised when using only sea level data because the exchange processes span a wide range of variability across the different dynamical regimes in our domain. Expendable bathythermograph (XBT) profiles and TOPEX/Poseidon (T/P) altimeter data are compared to temperature anomalies (TA) and to dynamic height anomalies (DHA) for the period 1993 through 1997 to determine how much can be inferred about the internal field of mass from sea level changes. Our focus is on the annual cycle along two well-sampled XBT sections on the western and eastern sides of the Atlantic Ocean from 10°S to 40°N. XBT profiles were matched (time/location) to Sea height anomalies (SHA) derived from T/P data, converted into DHA using TS relationships and then binned monthly into 2° of latitude by 4° of longitude boxes. The vertical mass distribution cannot always be inferred from SHA alone, unless there is a strong relationship between SHA and DHA and an understanding of the details of how temperature variability affects DHA. These relationships can be problematic if SHA are small. This occurs in zones of transition in the vicinity of troughs where small fluctuations in SHA belie the true nature of water column variability. These areas separate the mid-latitudes where surface buoyancy fluxes dominate from those in the equatorial region where ocean dynamics cause thermocline effects that dominate the forcing of sea level. Thus, the variability of SHA in transition regions tends to be small because both surface and thermocline variability may be significant but compensating in nature. This emphasizes how important direct observations (*in situ* data) can be in interpreting SHA correctly. Strong relationships between SHA and DHA are suggested where more than half of the SHA variance in the annual cycle can be accounted for by DHA (approximately 30% of the positions

Corresponding author. Tel 305-361-4345. Fax 305-361-4412. Email: molly.baringer@noaa.gov.

along the two XBT sections). These relationships between SHA and DHA for residual variability (obtained by removing the annual cycle) are weak. The exceptions are in two areas of large sea height variability in the western basin where there is significant interannual variability. The first is in the tropics in the vicinity of the tropical gyre trough near 50°W 8°N . The second is in the Gulf Stream near 70°W 38°N . An analysis of Panulirus data at (32.2°N , 64.5°W) suggests that *in situ* data may be needed down to at least 1000m where interannual variability accounts for about 40% of the SHA variance.

1. INTRODUCTION

Our objective is to investigate the relationship between the structure of upper ocean water column variability and its associated sea height anomaly (SHA). This is a critical issue when deriving inferences about the water column when only SHA measurements are available. In this paper, we focus on two well-sampled meridional sections in the western and eastern Atlantic Ocean that extend from 10°S to 40°N (Figure 1), where expendable bathythermograph data (XBT) data are most plentiful. The XBT locations are displayed on the mean 500m dynamic height field, which serves as a proxy for the geostrophic circulation field (Figure 1a). Both sections cross several dynamically distinct regions, e.g. in the tropics the seasonal North Equatorial Counter Current (NECC) and the tropical gyre and to form a basis of comparison, also across the northern subtropical gyre. The relationships between SHA and subsurface temperature variability can thus shed some light on where useful inferences about the subsurface mass field can be made in dynamically distinct regimes.

The variability of the upper ocean mass field, which is embedded in altimeter observations on large scales, has been studied using both surface observations and model results. Observationally, *Stammer* [1997] investigated the underlying causes of sea level variability in TOPEX/POSEIDON (T/P) data using surface observations and linear vorticity arguments applied to theoretical wind induced circulation changes. He found that in mid-latitudes, buoyancy fluxes dominate SHA variability, while in the tropics, vertical movements of the thermocline, caused mostly by changing winds and near-surface currents, dominates. Using numerical models, *Fukumori et al.* [1998] and *Ferry, Reverdin and Oschlies* [2000] (hereinafter FRO), found similar results using a combination of surface data and model fields. These findings are consistent with earlier studies of the oceanic thermal structure. For example, *Gill and Niiler* [1973] described the importance of seasonal variability of surface buoyancy fluxes on the mid-latitude temperature structure of the upper ocean. In contrast, *Merle and Arnault* [1985] discussed the importance of thermocline variability in forcing temperature changes in the tropics by virtue of wind-driven ocean dynamics. *Carnes et al.* [1990] and *Blaha and Lunde* [1992] compared inferred temperature profiles and sea height derived from Geosat observations to air deployed XBT data. The largest discrepancies between the two are found in regions of large

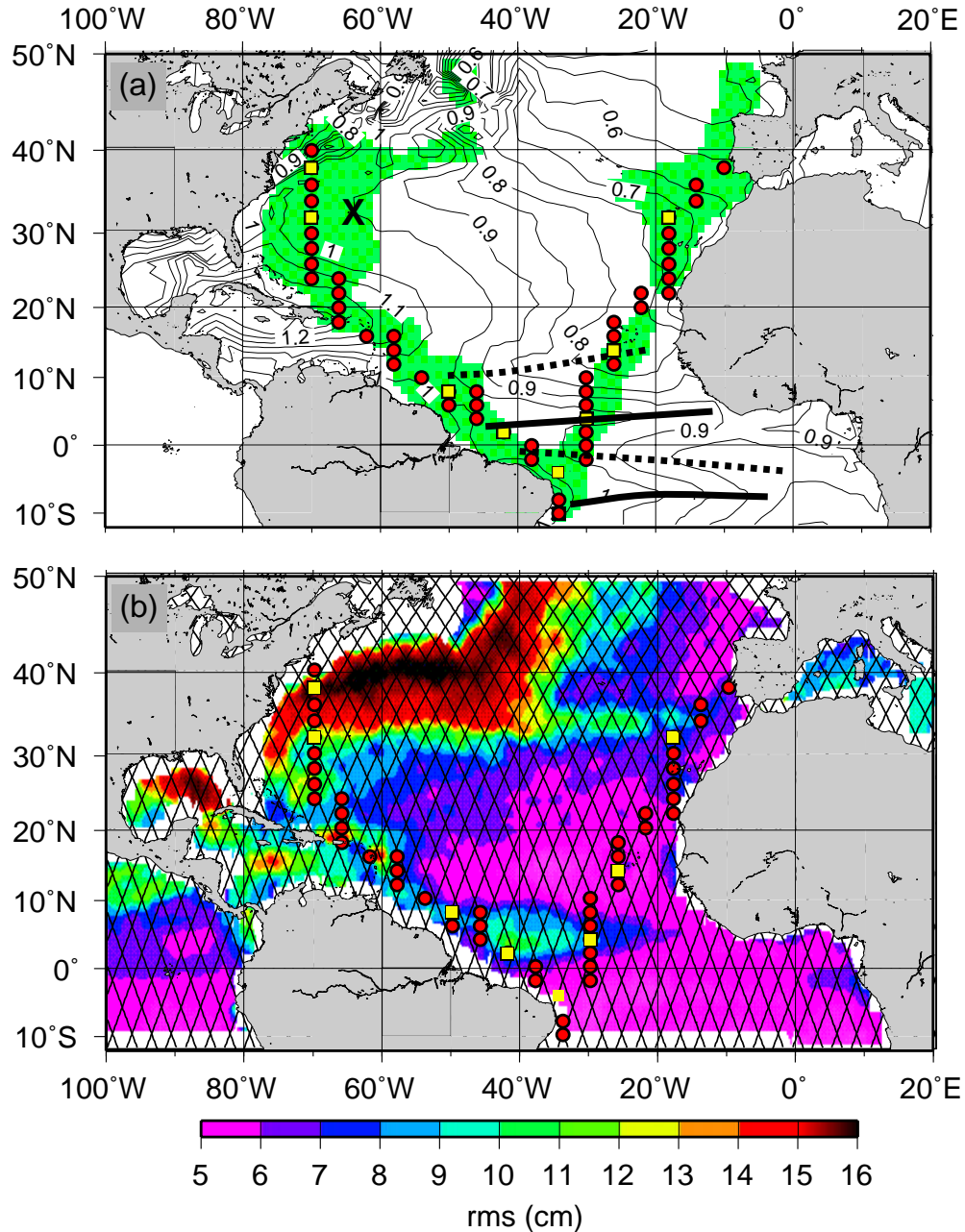


Figure 1. Two well-sampled western and eastern sections for expendable bathythermograph, (XBT) data denoted by large red dots and yellow boxes. These are positioned at the center of 2° of latitude by 4° of longitude boxes in which the data were binned. (a) Dark shading indicates areas of the highest density of profiles near major shipping routes where 30 months or more out of a possible maximum 60 months are available for the five years (1993-1997). The eight yellow boxes selected for detailed analysis have at least 41 months of data. The large dark cross indicates the location of the Panulirus station. The 500m dynamic height field is superimposed. Contour interval is 0.05 dynamic meters. The tropical ridges (heavy dark lines) and troughs (heavy dashed lines) are indicated. (b) Satellite tracks for T/P superimposed on the root mean square (rms) deviation of sea height anomalies (SHA).

horizontal gradients (differences occasionally exceeding 1.4 m). Using more reliable T/P data, *White and Tai* [1995] evaluated the role that T/P data can play in estimating upper ocean internal energy anomalies (note they called this heat content, see *Warren* [1999]) over large portions of the global oceans. They compared internal energy anomalies derived from interpolated XBT data to T/P SHA data and found good agreement on a global scale for the period 1993 to 1994. *Gilson et al.* [1998] compared T/P SHA signals to those found in an eddy-resolving XBT section across the subtropical North Pacific. They found that the 5.2 cm root mean square (rms) of the differences are scale dependent and dominated by scales longer than 500 km. Differences increase near the western boundary, however the signal to noise ratio also increases. They also found that the differences are smaller when *in situ* salinity data from expendable conductivity temperature depth probes were used instead of climatological salinity data.

Many authors have attempted to infer subsurface information from surface fields either through statistical means (e.g. *Hulburt et al.*, 1990) or through dynamical application of surface conditions within a model (e.g. *Cooper and Haines*, 1996). The combination of SHA derived from satellite altimeter data and *in situ* temperature and salinity data directly, should be a first step towards studying the dynamics of the upper ocean. In this paper, we show that *in situ* data, such as XBT data, used together with remote sensing data sets are essential to aid in modeling studies of ocean dynamics, climate forecasts and global sea level changes. Within this context, altimeter data combined with XBT data aid in the interpretation of the variability of the entire water column. In particular, the pathways of mass and heat between the South Atlantic and the North Atlantic across the complex equatorial region of zonal currents that is central in the exchange processes connecting the tropics and the subtropics, can be difficult to quantify if only altimeter data are used. *In situ* data are needed to interpret sea level changes in terms of how the structure of the upper ocean (density field) is organized. Disregarding tidal effects, changes in sea level can be caused by a combination of surface buoyancy fluxes and ocean dynamical adjustments, either baroclinically through subsurface density changes or barotropically.

In the analysis that follows we emphasize subsurface observations and examine in detail the vertical structure of the relationships between SHA and water column variability. Comparisons have been made between SHA from T/P data, TA profiles from XBT's and estimates of dynamic height anomalies (DHA). Because changes in sea level are a consequence of both surface fluxes and ocean dynamics (thermocline variability), we will show that these effects can act in opposition in certain transition regions of the Atlantic [*Mayer et al.*, 2001] to diminish the magnitude of sea level variability there. This chapter is organized as follows. The data sets are introduced in section 2. In section 3 the extent to which TA and DHA can be estimated from SHA data is investigated by means of a regression analysis. Although this work emphasizes the annual cycle (i.e., the

monthly means), the interannual variability is also considered. The inferences drawn from our analyses are discussed in section 4 and summarized in section 5.

2. DATA AND METHODS

Historical XBT profiles are not spaced uniformly. The highest density of profiles can be found along major shipping routes and in near-coastal regions. Consequently, for comparing time series of TA and DHA with SHA, XBT positions were chosen in areas (which we will term 'sections', though no single ship proceeds along these lines) with the most data along the western and eastern regions within the Atlantic (Figure 1a). XBT data was binned into a 2° of latitude by 4° of longitude boxes in order to compensate for the non-uniform distribution in space and time (Mayer *et al* 1998). There are 52 selected positions along both sections where the analysis was made. However, only approximately half of them (31) subjectively qualify for a detailed analysis by virtue of adequate temporal sampling (40 months out of a possible 60 months). Of these, the eight positions indicated by the yellow boxes in Figure 1 were selected as representative of the different regions of variability in the analysis domain.

The data sets of SHA, TA and DHA in the analyses and discussions that follow represent only departures (anomalies) from the mean background state. The mean background state is referenced to the five years 1993-1997 (the period in common for XBT and T/P data) and anomalies are computed over this time period. Units of DHA are scaled by 10/g, where g is the acceleration of gravity.

2.1. Hydrographic data

Along the two sections, there are 8012 individual XBT profiles, which were binned and then matched with the SHA data as explained below. Quality control procedures for the XBT data are given in *Molinari et al.* [1997]. Of the total number of profiles, only 60% reach a depth of 750m but 73% extend to 500m. Thus, to utilize as much data as possible a reference depth of 500m was chosen and unless otherwise stated, DHA values quoted herein are referenced to 500m.

Inferred DHA were derived by combining the XBT profiles with the salinity values determined from the local seasonal T versus S relationship obtain from the 1° x 1° Levitus monthly climatology [*Levitus* , 1982]. Issues concerning the effect of varying reference levels and errors induced by using climatological versus actual salinity profiles were estimated by using T,S profiles from the Panulirus station (32.2°N, 64.5°W) [*Talley and Raymer* , 1982]. While the Panulirus data is well outside the tropical Atlantic and will not contain the same sensitivity to salinity variability expected in the tropics, the time series provides the best available data to assess temporal variability without contamination from spatial variability.

2.2. Altimeter data

The spatial coverage by T/P is indicated by the satellite ground tracks (Figure 1b), which the satellite repeats approximately every 10 days. The along track resolution is 9 km and the separation between consecutive ground tracks is approximately 300 km on the equator. The altimeter data contain the standard corrections for wet and dry troposphere, earth and ocean tides [Cartwright and Ray, 1991], inverse barometer and sea state bias [Cheney *et al.*, 1994]. Altimeter errors, including environmental corrections, are estimated to be at worst only 5 cm for single-pass sea level measurements [Cheney *et al.*, 1994]. The SHA data were matched in both time and position to individual XBT profiles. Daily SHA gridded (0.1 degrees) fields were computed using a Gaussian interpolator of 0.5 degrees. The SHA value corresponding to each individual XBT observation was obtained by matching the closest SHA grid point to the XBT location. The SHA is then binned into the 2° latitude x 4° longitude boxes and averaged by month for the 5 year period (1993-1997) used as a reference for the sea height and dynamic height anomalies. The rationale for 2° x 4° binning is offered in Molinari *et al.* [1997]. For the Panulirus site (32.2°N, 64.5°W), the altimeter data were averaged within 1° of this location and were obtained from one descending altimeter ground track. Ascending and descending tracks improve the spatial resolution further [Le Traon *et al.*, 1990], with length scales that can be resolved by altimeter data well within the resolution of the 2° x 4° boxes. Although there are spatial and temporal limitations imposed by the number of XBT observations, all of the T/P data can be used. With all available T/P data in each of the 2° x 4° boxes, monthly means (annual cycle) were computed for comparison with the smaller matched set corresponding to the XBT data.

3. ANALYSIS

3.1. Background states and climatology

Although the mean background states of sea level and dynamic height cannot be compared because of uncertainties in the mean sea surface height field derived from T/P altimeter data, a geophysical context can be provided by superimposing the positions of the two western and eastern sections on the mean dynamic height field referenced to 500m (Figure 1a). This dynamic height field was derived using the TS relationship from the Levitus climatology as described above, together with the temperature climatology [Mayer *et al.*, 1998]. The circulation gyres of the mean geostrophic velocity field in terms of their temperature climatology and Sverdrup stream function have been studied by Mayer and Weisberg [1993]. These circulation gyres are consistent with the mean dynamic height field seen in Figure 1a, which shows the northern hemisphere subtropical gyre and the tropical gyre just north of the equator. The equatorial gyre, which straddles the equator, is not clearly indicated due in part to the failure of geostrophy close to the equator and the complicated vertical structure down to 500m [Mayer *et al.*, 1998]. Both sections can be seen to cross

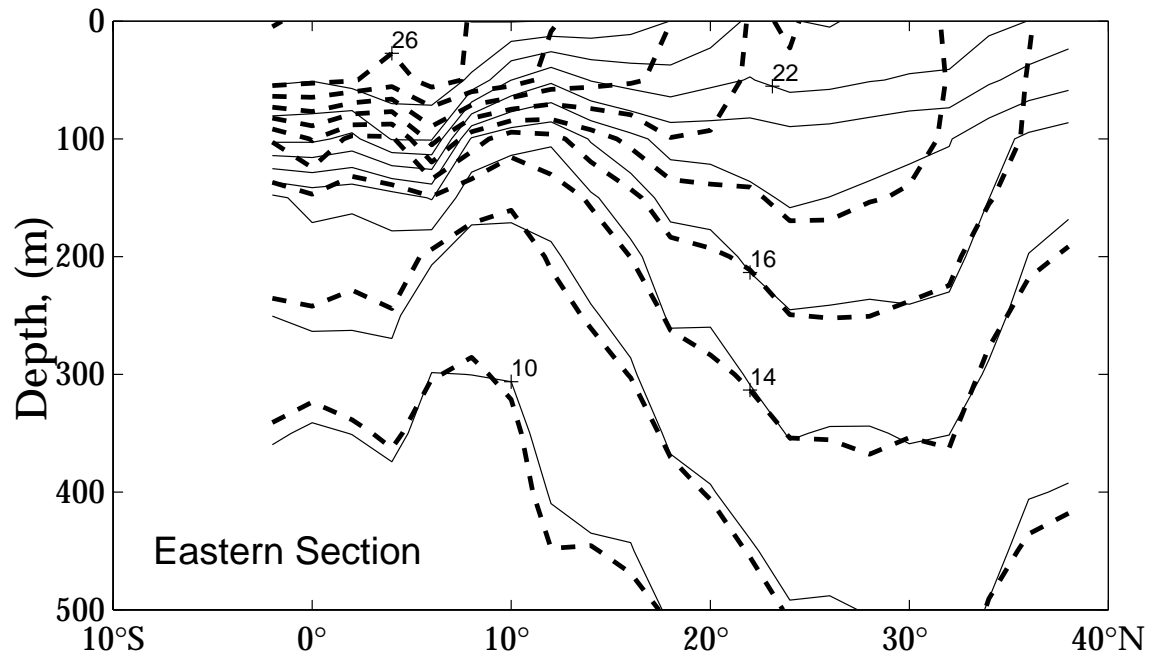
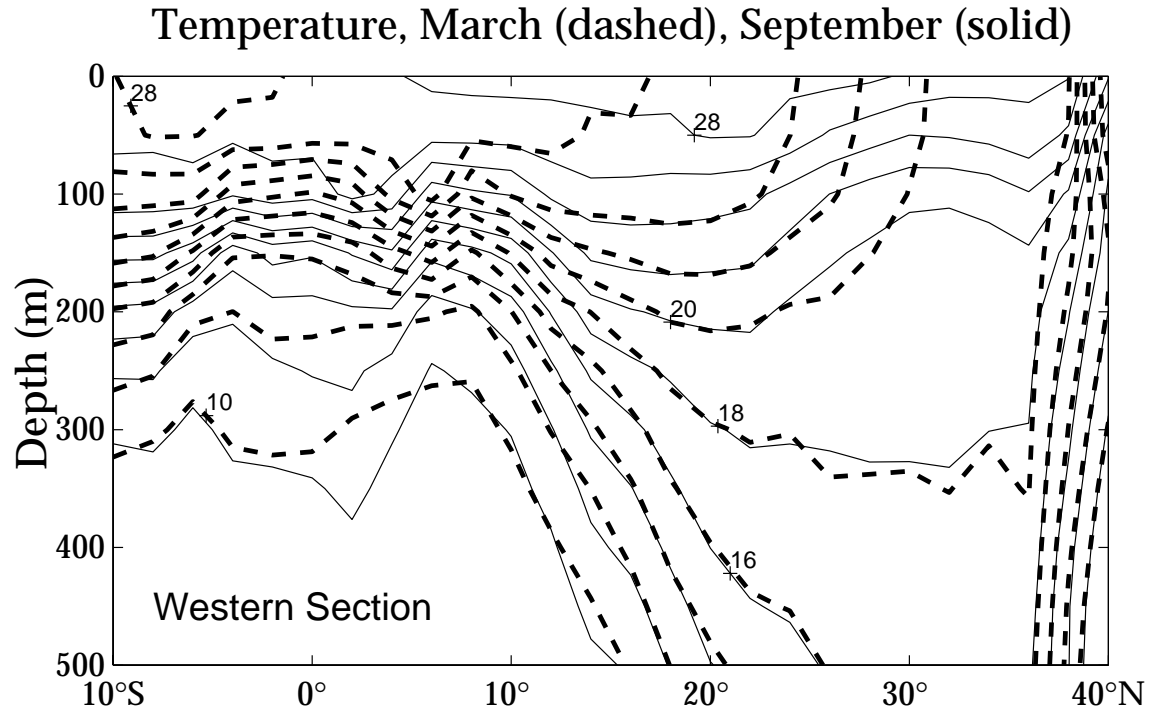


Figure 2. Seasonal extremes of temperature, March (dashed) and September (solid) for western (top panel) and eastern (bottom panel) sections ($^{\circ}\text{C}$) for the smoothed annual cycle (2 harmonic reconstruction). Contour interval is 2°C . Contour labels can apply to both dashed and solid contours when the contours are close together.

tropical and subtropical gyres and hence, are embedded in many different dynamical regimes that span a broad range of variability.

The variability of the circulation gyres is manifested as departures (anomalies) from the mean background state. Most regions in our domain have a reasonably large annual cycle. However, where the annual cycle is small, interannual variability and/or higher frequencies prevail (periods less than three months). These higher frequency fluctuations may be real or be caused by aliasing due to temporal and spatial sampling of XBT profiles. Recently, *Stammer and Wunsch* [2000] addressed the aliasing problem and suggested that barotropic aliasing is problematic in high latitudes. Along our sections however, their estimates of barotropic aliasing of SHA amount to no more than an rms of 2 cm. Henceforth, the term "residual" will refer to data from which the mean annual cycle has been removed. Thus, the "residual" contains both interannual variability and the higher frequencies just discussed. Qualitatively, the effects of the annual cycle on the field of mass can be obtained by looking at the seasonal extremes (March and September) of the western and eastern temperature sections (Figure 2). The seasonal extremes from a smoothed annual cycle were determined by reconstructing the temperature using only the annual and semiannual harmonics. A major difference between the winter and summer seasons are that in winter the isotherms slope almost vertically down from the surface south of 35°N in both sections. The seasonal cycle of temperature profiles in the tropics is evident in the thermocline along both sections. Thus, the largest variability is near the surface north of 20°N in the subtropics, while it is in the 50-200m depth range in the tropics from about 5°S to just north of 10°N. Using similar meridional sections *Mayer et al.* [1998] showed that most of the variability is captured in the upper 200-300 m of the water column.

For the eight representative locations (yellow boxes in Figure 1), the annual cycle of the TA profiles (Figure 3) and the temperature depth anomalies, the annual cycle and time series of SHA and DHA with respect to 500 m are examined here. In the tropics in the vicinity of and just north of the equator, the range of temperature that characterizes seasonal extremes is larger below the surface (Figures 3b and 3c and Figures 4b and 4c, middle panel). This is caused by the seasonal cycle of the zonal currents (wind-driven ocean dynamics) and their ridge-trough system (Figure 1a) manifest as changes in the depth of the thermocline. In the subtropics (Figures 3f-3h and Figures 4f-4h, north of 30°N), the range is larger near the surface and is a consequence of the annual cycle of surface buoyancy fluxes. Near the equatorial trough (Figures 3a and 4a, near 34°W 4°S) and in the vicinity of the North Equatorial Countercurrent (NECC) trough (Figures 3d and 4d, near 50°W 8°N and 3e and 4e near 26°W 14°N, as examples), there are competing influences due to a combination of both surface and thermocline variability that act in opposition. Here, surface and thermocline variability are negatively correlated and their contributions to SHA tend to cancel resulting in diminished SHA. Areas that are characterized by competing influences are termed in this work *transition regions* and exist between where

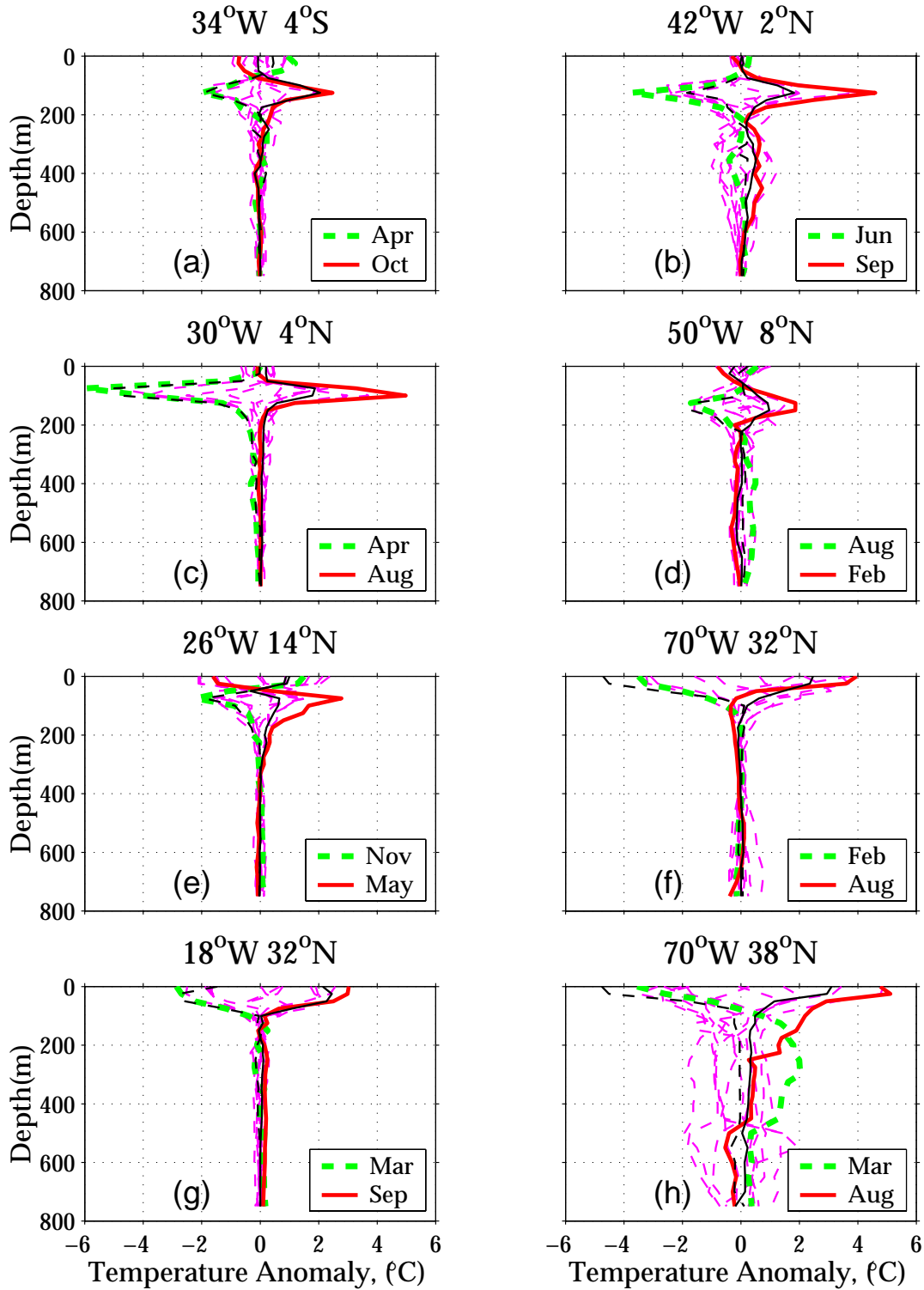


Figure 3. Profiles of temperature anomalies (TA) for eight representative positions indicated by the yellow boxes in Figure 1 for the annual cycle. The thick dashed green/solid red curves correspond to the minimum/maximum temperatures achieved for the month indicated in each legend. The thin black curves are the inferred TA profiles discussed in the text. The thin dashed purple curves are all other months.

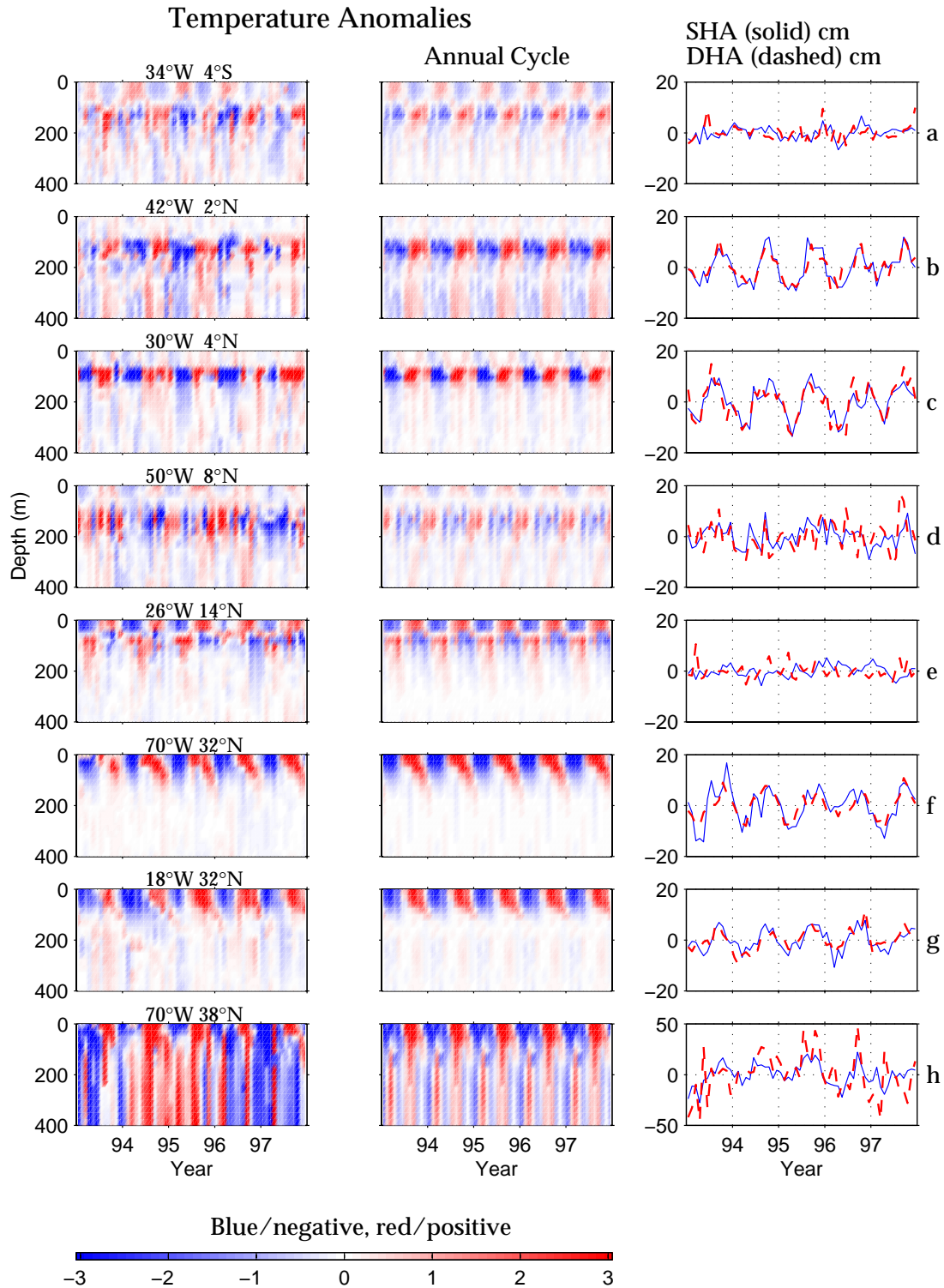


Figure 4. Depth dependence of temperature anomalies (TA) for the eight positions as in Figure 3 for the 5 yr period 1993 through 1995 (left panels), for the annual cycle repeated for 5 yr (middle panels), and time series of SHA and DHA with respect to 500m (right panels). Anomalies are negative (blue) positive (red). Missing data were filled with the annual cycle.

thermocline variability dominates SHA and where surface fluxes dominate.

In the immediate vicinity of the equator, complex processes that are related to equatorial upwelling also conspire to produce surface and thermocline variability that are negatively correlated but for reasons that differ from those in transition regions. Rossby and Kelvin waves affect the vertical temperature profile and thermocline depth and sea height (Franca et al, this volume). These waves deepen or raise the thermocline, where the deepening of the thermocline (downwelling) leads to a warming effect. The opposite takes place when the thermocline rises due to an upwelling event, thus leading to compensating effects on surface dynamic height.

3.2. Regression between SHA and TA and DHA

A linear regression scheme provides a description of the relationship between SHA and TA and DHA. For DHA with reference depths from 50-500m, correlation and regression coefficients are plotted in Figure 5. The linear approximation utilizes the SHA as the predictor or input, and the TA or the DHA as the predictand or output, thus relating a scaled delayed SHA to both TA and DHA. For TA,

$$TA(z,t) = r (SHA(t - \tau)) + \text{noise},$$

where $TA_m(z,t) = r(z) (SHA(t - \tau))$ is the modeled TA (and similarly for DHA). Hence the regression coefficients (r) have units of gain and are $^{\circ}\text{C cm}^{-1}$ if TA are the predictands and the time delay or lag (τ) is in months. These inferred TA profiles are also plotted along with the observed TA profiles in Figure 3. If DHA are the predictands, the units of gain are dyn. meters m^{-1} or dyn. centimeters cm^{-1} .

Questions about the spatial resolution of $2^{\circ} \times 4^{\circ}$ binning, involve whether or not the results presented here would have changed substantially if better resolution had been available. One region was densely sampled enough so that sensitivity to spatial resolution could be considered. In the western section sufficient data (64% of the total number of observations from the original $2^{\circ} \times 4^{\circ}$ box) are available in a 1° of latitude by 1.5° of longitude area centered at 70.25°W , 37.5°N . The same binning procedures were used as described above. The results are essentially the same as indicated by the large dot at 37.5°N in Figures 5a and 5c. Other regions however, lack the data density to consider the effects of spatial resolution.

3.3. Correlations

In the western section (Figure 5a) the correlations between SHA and DHA (with respect to 500m) south of the equator from 10 to 4°S in the equatorial gyre are low, in that they fall below the 90% confidence limit as determined by the

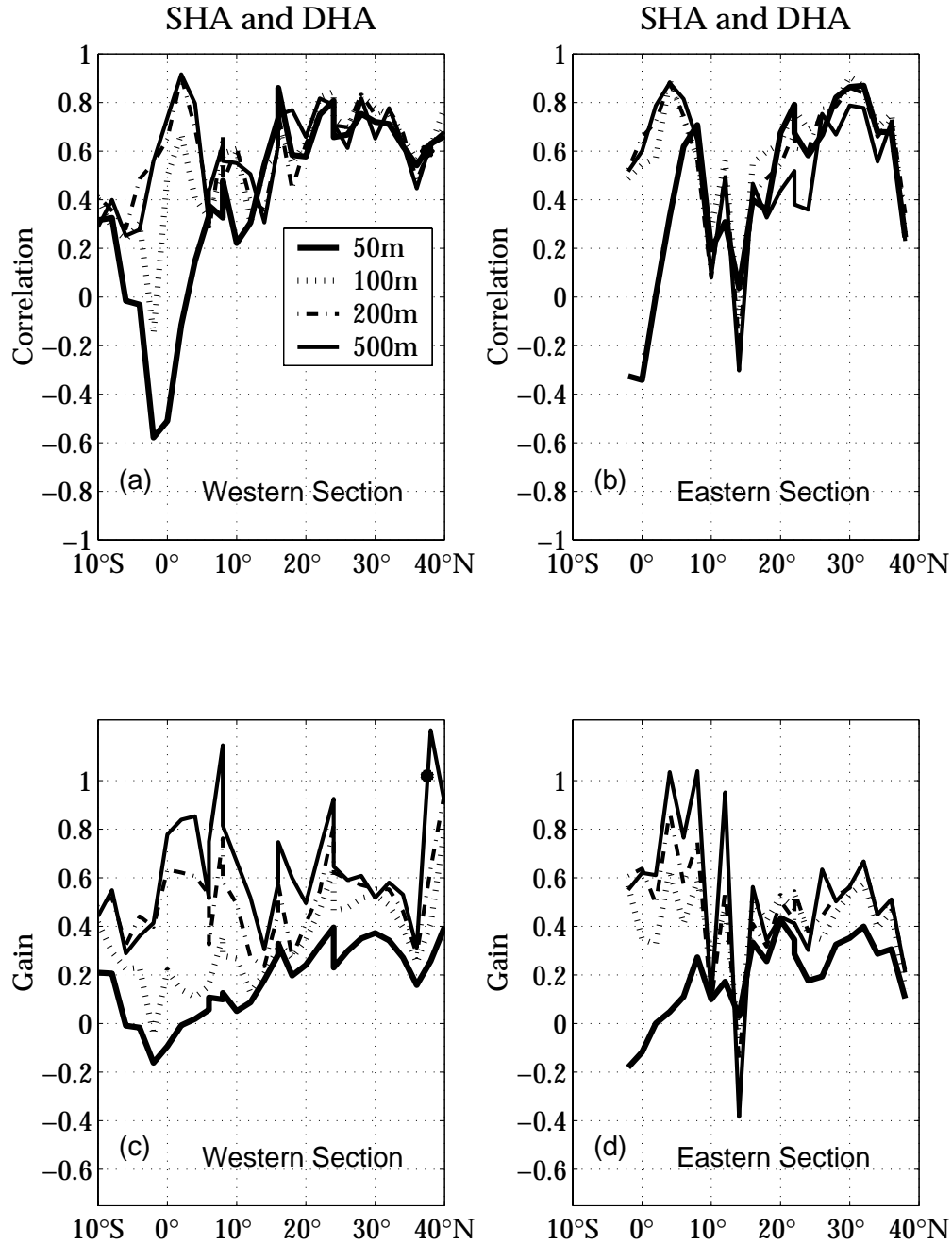


Figure 5. Correlations between sea height anomalies (SHA) and dynamic height anomalies (DHA) for (a) the western section and (b) the eastern section. Gains for (c) the western section and (b) the eastern section. SHA and XBT data were matched in time and space before binning by month in each 2° of latitude by 4° of longitude box. Curves for DHA are referenced to depths from 50m to 500m. Units for gain are dynamic meters m^{-1} or dynamic centimeters cm^{-1} . In the western section a separate analysis was performed on a 1° of latitude by 1.5° of longitude box centered at 70.25°W, 37.5°N. The resulting correlation and gain (a and c, respectively) are indicated by the large dot at 37.5°N.

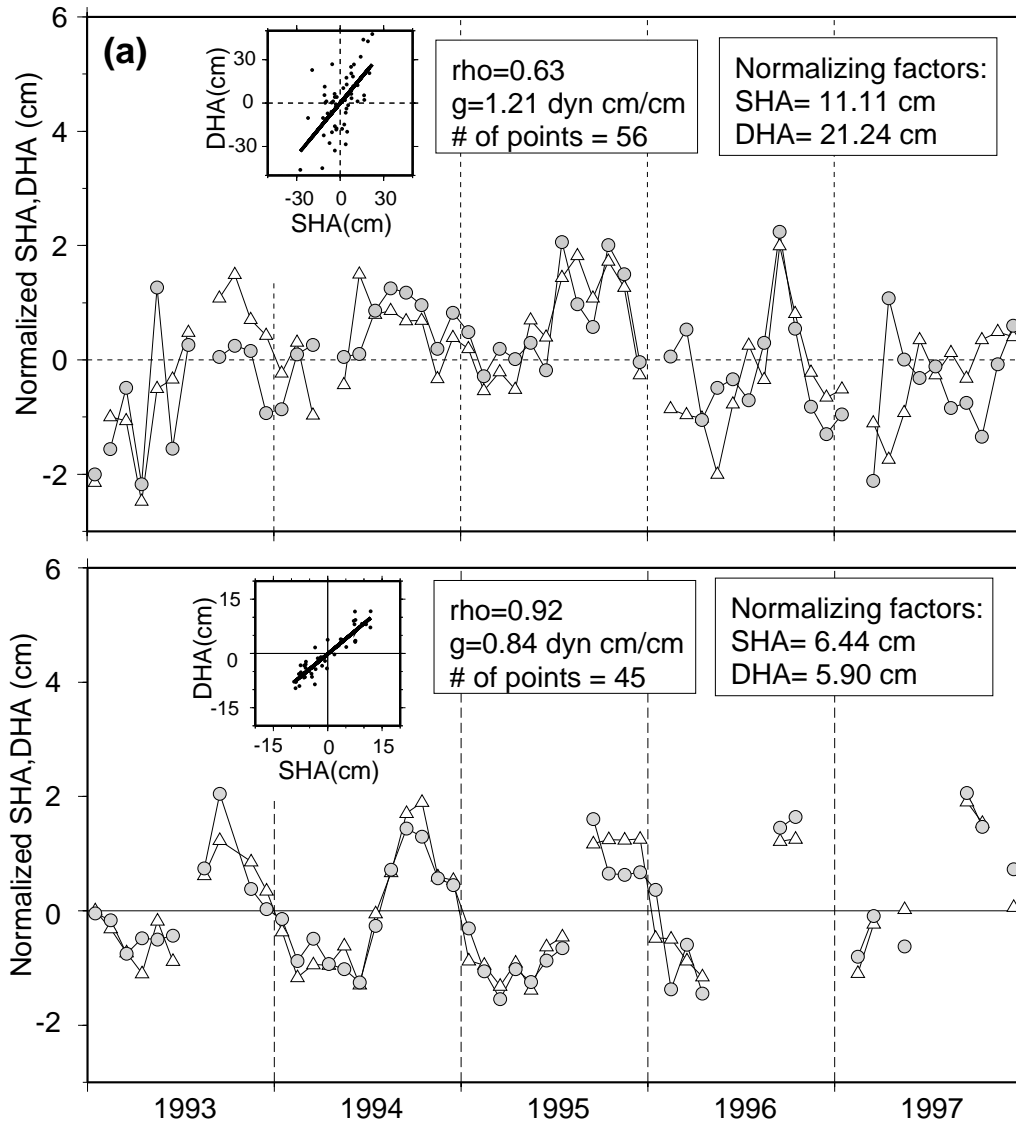


Figure 6. Sea height anomaly (SHA) and dynamic height anomaly (DHA) and their regressions (inset) at (a) 70°W 38°N and (b) 42°W 2°N. Time series of SHA and DHA are normalized by their standard deviations (rms values). To rescale the data multiply each of the time series by their corresponding rms values.

method of Sciremammano [1979], which accounts for serial correlation in the time series. They are also low in the tropical gyre near 6°N and again near 14°N just north of the tropical gyre axis in the region of the NECC trough and at 36°N in the subtropical gyre. The correlations are high within several degrees of the equator (0°-4°N) and in the subtropical gyre from about 16 to 34°N. In the eastern section (Figure 5b) correlations are low from about 10 to 24°N and at 38°N and negative near 14°N. The correlations are high just north of the equator in the southern part of the tropical gyre from 0 to 8°N and in the subtropical gyre from about 26 to 36°N. The reasons that the correlations between SHA and DHA

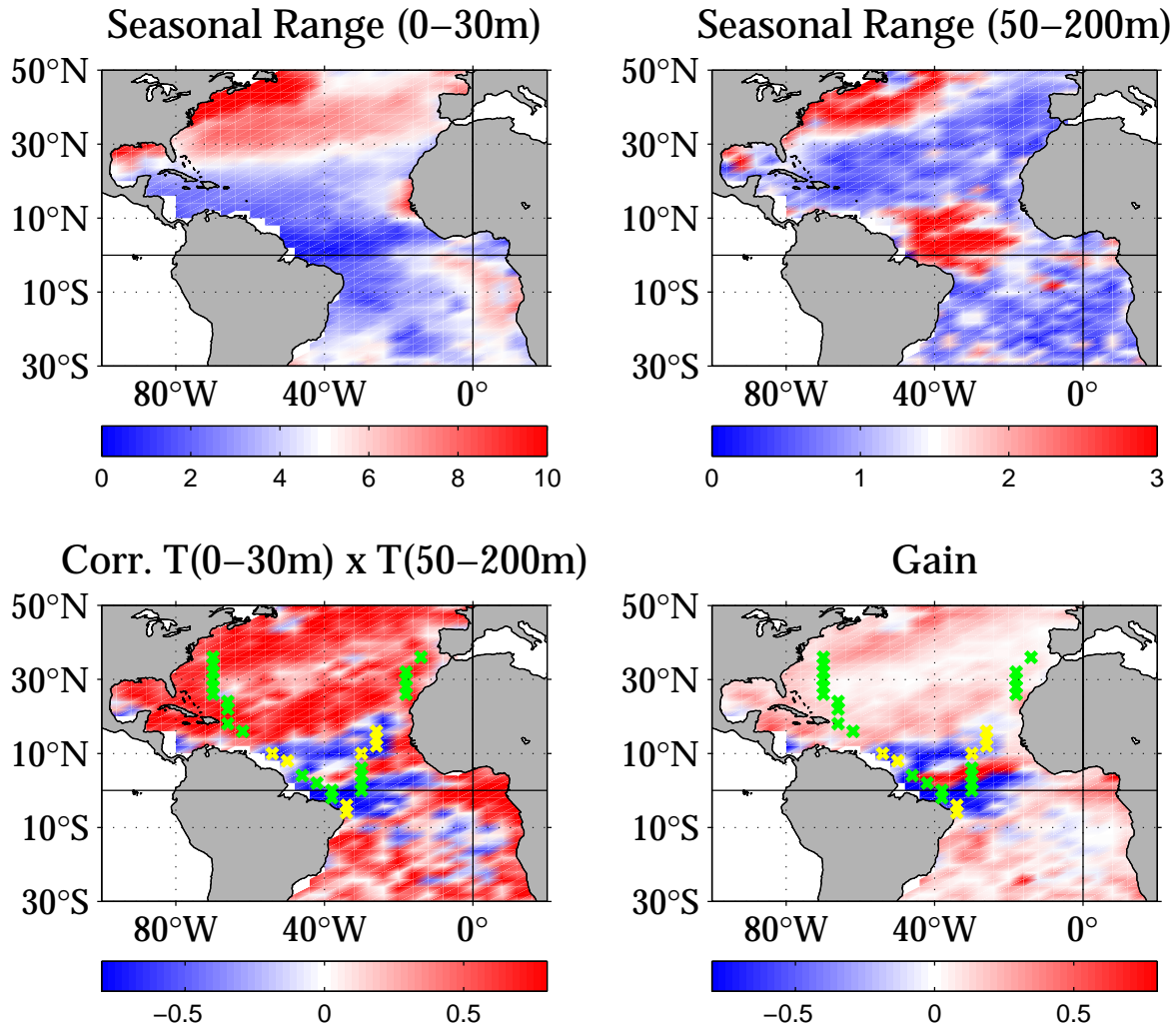


Figure 7. Seasonal range for indices of near surface (upper left panel, 0-30m) and thermocline (upper right panel, 50-200m) temperatures ($^{\circ}\text{C}$) and the regression between them. Lower left (right) panel shows the correlation (gain) field where the blue (red) are negative (positive). Also shown are green x's where DHA with respect to 500m can account for half or more of the SHA variance. Yellow x's denote transition regions.

are high or low depend on the details of how temperature variability in the water column relates to SHA. The relationship between the time series of SHA and DHA in some instances may not be straightforward, shown by the depth dependence of temperature and its relationship to SHA (Figure 4). These relationships can be complex and are generally problematic where SHA are small. Of particular interest is the importance of the annual cycle in the thermocline and how it affects the DHA from 4°S to 14°N (Figures 4a-4e, middle panels). Along the NECC ridge just north of the equator (Figures 4b and 4c), the thermocline variability is dominant and contributes the most to the DHA. The amplitude of the annual cycle is of roughly 7 dyn. cm in the vicinity of the NECC

ridge [Merle and Arnault, 1985]. This is consistent with the results of DHA (Figures 4b and 6b). In the transition region near 14°N (Figure 4e), the competing influences between surface and thermocline processes are offsetting in their contributions to DHA. Neither changes in thermocline depth or surface processes dominate the variability. Because of this, the areas of transition in the vicinity of trough regions have poor correlations that are intuitive after inspection of the TA with depth fields and the time series of SHA and DHA (Figure 4e). Farther north in the subtropics, surface processes are dominant and contribute most to the DHA. Near 32°N, there is a phase lag as a function of depth (Figure 4f). This lag is an artifact of temperature anomalies taken around a mean value and is due to the erosion of the seasonal thermocline through penetrative convection.

To appreciate how temperature changes of the upper ocean for the annual cycle co-vary with each other throughout the analysis domain, temperature range and unlagged correlations (Figure 7) between indices of near surface temperature over the upper 30m or so and the thermocline (50-200m) were computed from the 12 month climatology derived in Mayer *et al.* [1998]. The range fields provide definitive areas where surface and thermocline variability are important and are consistent with the discussions above, except that the whole domain is considered rather than just the two western and eastern sections. Surface variability is organized around the mean position of the Intertropical Convergence Zone. Thermocline variability is greatest in the tropics because of ocean dynamics in the vicinity of the equator and the NECC ridge and north of 30°N because of late winter convection (Figure 2). For the correlations and gains (lower panels), the negative shadings delineate the transition regions where surface and thermocline temperature indices are out of phase in the vicinity of the equatorial trough and the NECC trough and include the areas where correlations between SHA and DHA are small. The transition regions along both sections are indicated by the yellow **x**'s in Figure 7. Here, small SHA variability does not always mean that *in situ* variability is low; just that there are competing processes that diminish observed SHA as in Figures 3e and 4e. For instance, we know variability in the North Brazil Current Retroflexion region is high (Figure 1), however competing wind stress driven dynamics adjust the thermocline upwards during summer when surface heating is at a maximum. Directly on the equator correlations are negative in the west and positive in the east. However, there is no evidence of a simple relationship between SST and the thermocline [Weingartner and Weisberg 1991]. The physics entail SST and thermocline variations that are most closely controlled by ocean dynamics when the thermocline is adjusting to basin-wide seasonal changes in the wind stress field. Franca *et al.* (this volume) show that Kelvin and Rossby waves can have substantial amplitude at annual period that in turn effect sea height and thermocline depth.

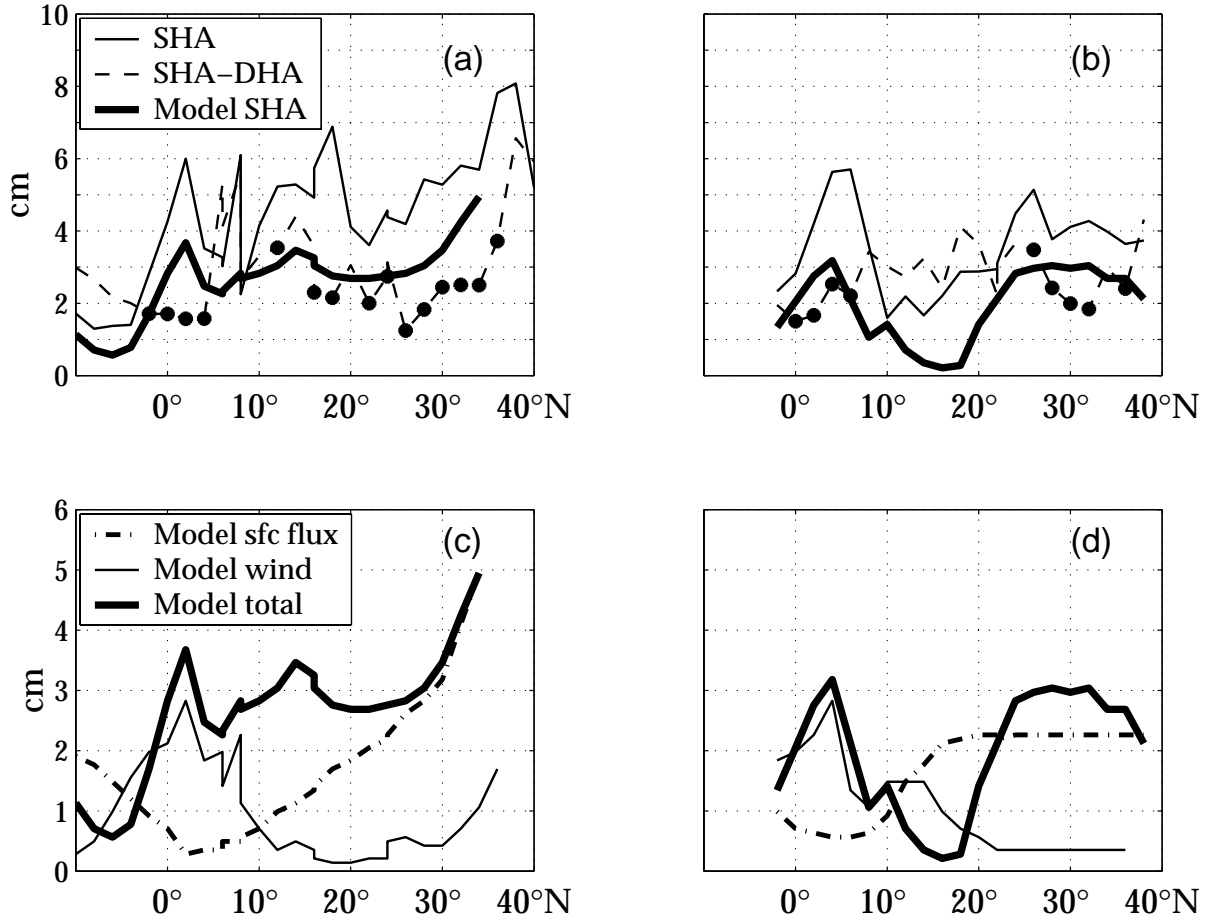


Figure 8. The root mean square (rms) deviation of sea height anomaly (SHA, solid), the differences between SHA and DHA with respect to 500m (dashed) for the annual cycle and model results (thick) from *Ferry et al.* [2000] for the annual harmonic only (a) in the western section and (b) the eastern section. The large dots on the differenced curves show where DHA with respect to 500m can account for half or more of the SHA variance. c) Model rms from heating/cooling and wind-driven components shown separately and their sum for the western section and d) the eastern section.

3.4. Variance explained

The amount of variance explained for TA or DHA by scaled delayed SHA, is obtained by squaring the correlations. Representative time series of SHA and DHA from two of the eight locations in Figures 1, 3 and 4 along with their regressions are shown in Figure 6, one in the tropics (Figure 6a, 42°W 2°N) where maximum variability is in the seasonal thermocline and another in the Gulf Stream (Figure 6b, 70°W 38°N) where most of the variability is near the surface. For the most part, the correlations are marginally significant with respect to a 90% significance level for the null hypothesis determined by the method of *Sciremammano* [1979], which accounts for serial correlation in the time series.

The correlations will vary according to the integral timescale determined by the effective degrees of freedom (DOF), which is always less than the length of the time series. Finally, there are no significant lags that improve the correlations between SHA and DHA (i.e., $\tau=0$). As will emerge below, correlations are best away from transition regions and where the annual cycle is a significant component of the variability.

To further explore the issues of inferred upper ocean structure for the annual cycle, there are locations where DHA can account for a large fraction of the SHA variability. Although somewhat arbitrary, these locations have been chosen where the rms of the differences (SHA minus DHA) reduces the variance of SHA by 50% or more (i.e., for a 50% reduction, the ratio [rms of the difference]/[rms of SHA] less than or equal to 0.707). The rms curves and the rms of the differences were computed for both the annual cycle (Figure 8) and then for the residual variance of SHA for the annual cycle is reduced by 50% or more and are also indicated by the green x's in Figure 7. These include four of the eight positions in Figures 3 and 4 (Figures 3b, 3c, 3f, 3g and 4b, 4c, 4f, 4g) and are candidates for deriving inferred TA profiles (Figure 3). The computation entails computing the regression coefficient (gain) and lag (time delay) between the SHA climatology for a particular location and the temperature climatology at that same location as explained above. Thus, the inferred TA profiles are just a scaled delayed SHA. In contrast, once the annual cycle has been removed the rms of the differences between residual SHA and DHA values (not shown) indicate that the variability of SHA generally can not be accounted for by DHA anywhere along the sections. Moreover, the importance of the annual cycle to the correlations is underscored when the correlations are derived from the residuals. With few exceptions they are no longer significant at the 90% SL and generally degrade substantially after removing the annual cycle. The few exceptions are important because these occur where interannual activity of some significance occurs. This occurs in the vicinity of 50°W 8°N (Figure 4d) and near 70°W 38°N (Figure 4h). There are some noteworthy features that these locations have in common. The annual cycle variance is less than the residual variance and the correlations are relatively unaffected by removing the annual cycle. Near 50°W 8°N, the residual profiles (not shown) indicate that interannual variability is similar in amplitude and is confined to approximately the same depth range (50-200m) as that for the annual cycle (Figure 3d). Further, there is a warming trend that extends from 2/94 to 12/95 (Figure 4d). Farther north at 70°W 38°N, the residual profiles (not shown) are relatively independent of depth and contrast with the maximum variability for the annual cycle, which is near the surface (Figure 3h). Also, the residual temperatures increase from 1/93 to 12/95 (Figure 4h).

3.5. Panulirus data and reference levels

The Panulirus data provide an opportunity to consider the relationship between SHA and DHA down to depths of 2000m. The Panulirus station in

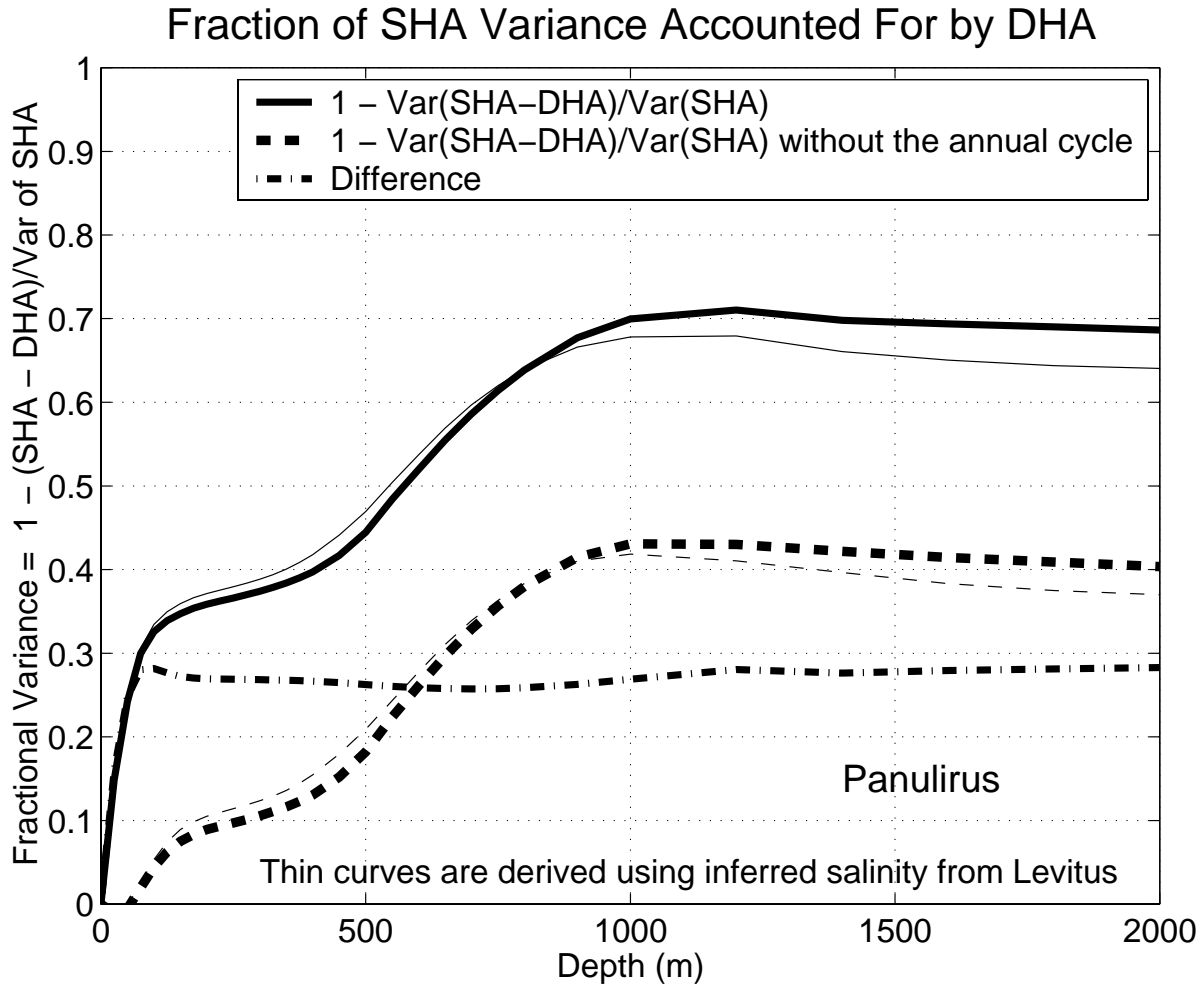


Figure 9. Fraction of SHA variance (fractional variance, FV) accounted for by DHA for the five-year period (two thick curves) including the annual cycle (blue), without the annual cycle (red) and their difference (green). Thin blue (red) lines represent the fractional SHA variance explained by DHA computed using climatological salinity with (without) the annual cycle.

located at 32.2°N, 64.5°W [Talley and Raymer, 1982]. Calculations were carried out down to 2000m to fully exploit the available data in ways that were similar to those using only XBT data. The altimeter data were obtained within 1° from the Panulirus location. Therefore, questions about DHA in the deeper parts of the water column can now be addressed that could not otherwise, had only XBT data been available. Although the amount of data available at the Panulirus station does not exist elsewhere, it does provide some perspective in allowing a more detailed examination of the relationship between SHA and DHA throughout the water column. The salient points here relate to the depths of annual cycle variability and residual variability. The latter is effectively the interannual component of variance and higher frequency fluctuations discussed earlier.

Using the hydrographic data, the two thick curves in Figure 9 are the fraction of SHA variance (fractional variance, FV) accounted for by DHA for the five-year period:

$$F_v = 1 - \text{variance (SHA-DHA)} / \text{variance (SHA)}.$$

One of the curves includes the annual cycle and the other is for the residual alone. Also plotted is their difference that is essentially independent of depth below 100m. The difference curve shows, that in the vicinity of Panulirus, the annual cycle is effectively limited to the upper 100m (see also Figures 3f and 4f) and accounts for a little less than 30% of the SHA variance. The annual cycle is also limited to the upper 100m across the whole basin at this latitude (32°N) as indicated by an analysis (not shown) of the temperature climatology from *Mayer et al.* [1998]. For the residual variability, the DHA below 100m continue to account for a larger and larger fraction of SHA variance down to about 1000m. The implication here is that near this location, residual variability (i.e. with the annual cycle removed), which includes interannual variability, is a factor that accounts for a little more than 40% of the total variance at 1000m. Together with the annual cycle, the total variance accounted for is about 70% near 1000m. If the DHA were to perfectly match SHA at some reference depth, then the thick solid curve would approach unity at that depth.

Although interannual variability at Panulirus is not well characterized by such a short record of only 5 yr, it is significant that essentially all of the SHA variance that can be accounted for by DHA is accounted for as a depth of 1000m is reached. Similar results were found by *Roemmich* [1990], who used an EOF analysis on Panulirus data alone. He found that the first EOF associated with the annual cycle, contains a surface maximum in the upper 100m. For yearly anomalies a secondary maximum is near 800m that decreases to negligible values below 1300m. Further, the results concerning correlations and gains (not shown) are consistent with those in Figure 9 in that values level off when nearing 1000m. The correlations with and without the annual cycle are both significant at the 90% SL.

3.6. Inferred salinity vs. *in situ* salinity

One of the shortcomings of our analyses relates to the lack of *in situ* salinity data. Questions arise over how estimates of DHA are compromised by using seasonal TS from the Levitus climatology [*Levitus* , 1982]. This issue was addressed by performing calculations using the Panulirus data described above in ways that were similar to those using only XBT data. The goal was to evaluate the effects of including *in situ* salinity against those obtained using inferred salinity as if the *in situ* data were not available. As described in section 2, inferred salinity was derived from the 1° x 1° Levitus climatology.

The most telling results from our inquiry into the effects of salinity is provided by the fractional variance curves in Figure 9. The fractional variance using inferred salinity (the two thin curves) is approximately the same magnitude as that using *in situ* salinity (the two thick curves). Although not shown, the rms of the difference (SHA-DHA) using *in situ* salinity versus using

inferred salinity is less than 0.5 cm at 2000m. However, the Panulirus station is in a benign region of ocean variability, e.g. away from strong gradients, fronts, etc. unlike some others in our analysis domain. As pointed out by *Gilson et al.* [1998], errors on scales of 1000 km and more increase from 0.5 to 2.4 dyn. cm when salinity sampling is absent. Moreover, there are locations in our domain where DHA using inferred salinity from the Levitus climatology would be impacted by high variability of Amazon water in the vicinity of 6°N in the western section. Thus, whether or not the results from Panulirus data apply elsewhere in the analysis domain is an open question and one that cannot be addressed with the available data. Despite this, these findings are encouraging and suggest that using seasonal TS in deriving inferred salinity is a reasonable approach.

3.7. Barotropic component

Our ability to assign the fraction of SHA that is barotropic depends on obtaining accurate estimates of the baroclinic component and may be compromised by the uncertainties that relate to the computation of the regression coefficient (gain). The unlagged baroclinic component of SHA is: $DHA_m(t) = r (SHA(t))$, where r is the gain. The calculation that provides the 90% significance level for the correlations also provides the number of DOF. The DOF are in a range from about 5 to 20 DOF and so a 90% confidence interval can be computed. For a gain of unity and $DOF \approx 10$, the true value (r) is very roughly $0.3r' < r < 1.3r'$, where r' is the estimated gain. Thus, with such large error bars the ability to assign the fraction of SHA that is barotropic is problematic.

In an ideal baroclinic ocean, if the internal pressure field completely compensates for the external field, the regression coefficient (gain) would be unity, the barotropic component of SHA would be zero and the DHA would match the SHA exactly. However, XBT analysis only allows DHA computations to 500m, thus leaving an unknown baroclinic component of the SHA below 500 m. By a rather wide margin in some places, gains computed herein are substantially less than one (Figures 5c and 5d), with values typically ranging from about 0.5 to 0.9 dyn m m⁻¹. In the Gulf Stream region, these gains compare favorably with the 0.8 dyn m m⁻¹ value obtained by *Blaha and Lunde* [1992] using Geosat data. These gains imply that barotropic variability is between 10-50% of the baroclinic variability. The gains are also consistent with the results of *Hallock et al* [1989] who found the average magnitude of barotropic fluctuations to be 30-50% of the baroclinic variability. Although we should be able to assign the fraction of SHA that is barotropic by virtue of knowing that the baroclinic fraction of SHA is equal to the modeled DHA (DHA_m), the errors discussed above that relate to the computation of the gain may seriously compromise this estimate. Observational studies, such as the *Meinen* [2001] study of the North Atlantic Current, have showed that the baroclinic and barotropic components of the transport are often only weakly correlated. *Hurlburt et al* [1990] also showed from a model and altimetry that the subthermocline pressure field can have significant impacts on SHA.

4. DISCUSSION

We investigate here the water column variability in terms of SHA and the relationships between SHA, TA and DHA fields. The central issue relates to the question of how much information can be inferred about the upper water column temperature field given only satellite altimeter data. These relationships can be complex and are generally problematic where surface and thermocline variability in transition regions are compensating in nature causing diminished SHA.

Several earlier studies have used numerical models and observations to address the relationships between SHA obtained from satellite altimetry and subsurface variability. For example, *Stammer* [1997] used three years of global T/P data to relate SHA to surface wind and buoyancy flux anomalies. Later, *Fukumori et al.* [1998] used a numerical model forced by daily winds and monthly surface fluxes over a period from January 1992-January 1994. Both studies concluded that in mid-latitudes, short time scale sea level changes are driven primarily by surface buoyancy fluxes. The results presented herein provide more detail on the vertical structure of the relationships between SHA and water column variability than provided in these earlier studies. North of 20°N, these newer results are consistent with those of *Stammer* [1997] and *Fukumori et al.* [1998].

More recently, FRO, using a combination of numerical model results and observations, studied the processes responsible for the observed annual cycle in a 5-yr T/P record in the Atlantic Ocean north of 10°S (Figure 8). Generally, the rms of the FRO model are akin to those from the observations suggesting that the model is simulating the processes that cause SHA. However, the model underestimates the rms of the observations because only the annual harmonic is considered. The contributions to the annual cycle by the simulated (modeled) buoyancy flux and wind forcing are given separately in Figures 8c and 8d. FRO considered air-sea fluxes, advection, salt content variability, water column variability at depths greater than 150 m and bottom pressure variability as potential candidates for possible forcing mechanisms of SHA. Similar to the results described above for SHA, FRO found that for the annual cycle, there is "an approximate balance between the air-sea heat flux induced changes in TA and DHA and SHA variability" in most regions north of 20°N. Our results are consistent with the FRO findings north of 20°N where surface buoyancy fluxes dominate the annual cycle of SHA but south of about 10°N, wind forcing dominates. Here, FRO found that near surface variability plays a much smaller role in the forcing of the annual cycle of SHA in the tropics where advective water column variability at depths greater than 50m become important. These findings are expected based on the recent analyses of *Franca et al* (this volume) and the analysis of the equatorial thermocline response to wind forcing during the SEQUAL Program by *Weisberg and Tang* [1990]. This chapter identifies the heretofore undescribed transition regions that tend to occur in the vicinity of

trough regions and cautions about such simple characterizations of DHA and SHA variability near the tropics.

In the tropics the range of temperature is largest below the surface and is caused by wind-driven ocean dynamics that lead to changes in the depth of the thermocline. In the subtropics the range of temperature is largest near the surface and is caused by surface buoyancy fluxes. Between these regions, the results in Figures 3, 4 and 7 indicate the presence of a transition between the subtropics and the tropics that are generally found in trough regions (NECC and equatorial troughs). Here, surface and thermocline variability are offsetting in their contributions to DHA resulting in diminished SHA and the thermocline is essentially out of phase (negatively correlated) with the annual cycle at the surface (as an example see Figures 3e and 4e at 26°W 14°N). In these areas the small changes in SHA are not particularly well suited for drawing inferences about changes in the subsurface temperature structure. Here, correlations are generally poor between SHA and TA and DHA and although the changes in SHA are small, *in situ* variability can be large. Compensation is caused by a deep (shallow) trough and shallow (deep) thermocline and warm (cold) water near the surface in concert with diminished (enhanced) surface fluxes due to seasonal relaxation (excitation) of winds. Negative correlations are also found along the equator in the western part of the domain, where equatorial upwelling induced by Kelvin and Rossby waves create a complicated picture for interpreting SHA and thermocline correlations.

Our ability to consider interannual variability met with marginal success because of the limited time span of our data (5 yr) and because of the number of missing data. The residual signals, which were obtained by removing the annual cycle, contain both interannual variability and higher frequencies. The largest interannual variability occurs in two areas along the western section. The first is in the tropics in a latitude band from 6 to 14°N. The second is in the Gulf Stream near 70°W 38°N.

In the tropics along both sections, residual variability is confined to a depth range of 50-200m in the thermocline and is approximately the same as that for the annual cycle. Just northwest of the retroflection region between 5 and 10°N and west of 46°W, intermittent currents occur along with the passage of rings shed by the North Brazil Current [*Didden and Schott, 1993*]. Recent fieldwork (*Garzoli, this volume*) revealed a much smaller SHA signature than the related DHA in observations of a specific ring. These recent observations are consistent with our results in this area for which larger rms of DHA were observed. Some of these rings have been reported to have a very deep velocity structure (>500 m) [*Richardson and Schmitz, 1993*] and therefore, for comparing DHA with SHA, reference depths of 500m or more would be needed. In the Gulf Stream region near 70°W 38°N, ocean variability is characterized by meanders and rings [*Hansen, 1970*]. Specifically, residual variability is important throughout the upper 500m and is largest at levels below the seasonal thermocline unlike the surface intensified annual signal. This depth structure of variability indicates that subsurface anomalies as well as anomalous surface

fluxes are responsible for SHA and DHA signals at interannual time scales. Further, an analysis of Panulirus data, only about 5°S of the Gulf Stream, also showed how important residual variability can be in causing SHA down to depths of 1000m or so, well below the seasonal thermocline.

Recently *Rossby and Benway* [2000], related surface salinity residuals to meridional movement of the Gulf Stream along a track between New Jersey and Bermuda (adjacent to the Panulirus station). This track crosses the western section near 70°W 38°N where the residuals are salty and TA are warm during mid-yr in 1995 and residuals are fresh and TA are cold in the beginning of 1997. This coincides with decreasing DHA over this time period (Figures 4h and 6a) and is consistent with southward movement of the Gulf Stream. Hence, the observed TA are directly related to ocean dynamics.

5. SUMMARY

The results presented herein support those from earlier studies which indicate that SHA must be used together with *in situ* data to interpret altimetric observations. It has been shown that the vertical mass distribution cannot always be inferred from SHA alone, unless there is a strong relationship between SHA and TA and DHA and an understanding of the details of how temperature variability affects DHA. These relationships can be problematic if the variability of SHA is small even though water column variability may be large. This can occur in areas of transition that are commonly found in trough regions (NECC and equatorial troughs) between the tropics and the subtropics where surface and thermocline variability of the annual cycle are offsetting (out of phase) in their contributions to DHA.

To draw inferences about the upper water column given only satellite altimeter data (SHA) from T/P, an attempt was made to derive inferred TA profiles based on the linear correlation between SHA and the annual cycle of TA over the range of depths available. The calculations are only applicable to the annual cycle because correlations are generally poor for the residuals. Candidates for this calculation are suggested where the variance (rms squared) of the difference between SHA and DHA is less than half that of the variance of SHA (Figures 7 and 8). At these locations (a little more than 30% of the available positions) more than half of the SHA variance in the annual cycle can be accounted for by DHA. However, computing inferred profiles becomes difficult in locations where the SHA have small values in transition regions for reasons stated above, for example near 26°W 14°N (Figures 3e and 4e).

For the annual cycle the most important contributions to SHA in the tropics are TA in the 50-200m depth range, and in the subtropics TA in the upper 100m. Using data down to 2000m from the Panulirus station (32.2°N, 64.5°W), it was found that residual water column variability can be important in contributing to the observed SHA below depths of 500m and that *in situ* data are needed down to at least 1000m. The inference may be drawn here that this situation may apply elsewhere as well. From Figure 9 it is evident that the

annual cycle at Panulirus is effectively limited to the upper 100m or so and accounts for almost 30% of the SHA variance. For the residual a little more than 40% of the SHA variance is accounted for by the DHA as a depth of 1000m is reached and is likely due mostly to interannual variability.

Acknowledgments

This research has been funded by NOAA's Office of Atmospheric Research and the Office of Global Programs. The authors are indebted to Yeun-Ho Daneshzadeh for her efforts in quality control of the XBT data, and to Chunzai Wang, Don Hansen, and Sonia Bauer for their thoughtful comments on this manuscript. The authors would also like to thank Bob Cheney (NOAA/NESDIS) for providing the altimeter data and Dr. Ichiro Fukumori for providing data from his model results.

References

- Blaha, J., and B. Lunde, Calibrating altimetry to geopotential anomaly and isotherm depths in the western North Atlantic, *J. Geophys. Res.*, **97**, 7465-7477, 1992.
- Carnes, M., J. Mitchell, and P. de Witt, Synthetic temperature profiles derived from Geosat altimetry: Comparison with air-dropped expendable bathythermograph profiles, *J. Geophys. Res.*, **95**, 17979-17992, 1990.
- Cartwright, D. E. and R.D. Ray, Energetics of global ocean tides from Geosat altimetry, *J. Geophys. Res.*, **96**, 16897-16912, 1991.
- Cheney, R. L. Miller, R. Argreen, N. Doyle, and J. Lillibridge, TOPEX/POSEIDON: The 2-cm solution, *J. Geophys. Res.*, **99**, 24555-24564, 1994.
- Cooper, M. and K. Haines, Altimetric assimilation with water property conservation. *J. Geophys. Res.*, **101**, 1059-1077, 1996.
- Diden, N., and F. Schott, Eddies in the North Brazil Current by Geosat altimetry, *J. Geophys. Res.*, **98**, 20121-20131, 1993.
- Ferry, N., G. Reverdin, and A. Oschlies, Seasonal sea surface height variability in the North Atlantic Ocean, *J. Geophys. Res.*, **105**, 6307-6326, 2000.
- Fukumori, I., R. Raghunath, and L. Fu, Nature of global large-scale sea level variability in relation to atmospheric forcing: A modeling study, *J. Geophys. Res.*, **103**, 5493-5512, 1998.
- Gill, A. E. and P. P. Niiler, The theory of the seasonal variability in the ocean, *Deep-Sea Res.*, **20**, 141-177, 1973.
- Gilson, J., D. Roemmich, B. Cornuelle, and L-L Fu, Relationship of TOPEX/POSEIDON altimetric height to steric height and circulation in the North Pacific, *J. Geophys. Res.*, **103**, 27947-27965, 1998.
- Goni, G., S. Kamholz, S. Garzoli, and D. Olson, Dynamics of the Brazil-Malvinas Confluence based on inverted echo sounders and altimetry, *J. Geophys. Res.*, **101**, 16273-16289, 1998.

- Hallock, Z. R., J. L. Mitchell and J. D. Thompson, Sea surface topographic variability near the New England seamounts: An intercomparison among insitu observations, numerical simulations and Geosat altimetry from the regional energetics experiment. *J. Geophys. Res.*, **94**, 8021-8028, 1989.
- Hansen, D. V., Gulf Stream meanders between Cape Hatteras and the Grand Banks, *Deep-Sea Res.*, **17**, 495-511, 1970.
- Hurlburt, H. E., D. N. Fox and E. J. Metzger, Statistical inference of weakly-correlated subthermocline fields from satellite altimeter data. *J. Geophys. Res.*, **95**, 11375-11409, 1990.
- Le Traon, P. Y., M. C. Rouquet, and C. Bossier, Spatial scales of mesoscale variability in the North Atlantic as deduced from Geosat data, *J. Geophys. Res.*, **95**, 20267-20285, 1990.
- Levitus, S., Climatological atlas of the world ocean, *Noaa Technical Paper 13*, 173 pp., *U.S. Government Printing Office*, Washington, D.C., 1982.
- Mayer, D. A., R. L. Molinari, M. O. Baringer, and G. J. Goni, Transition regions and their role in the relationship between sea surface height and subsurface temperature structure in the Atlantic Ocean, *Geophys. Res. Lett.*, **28**, 3943-3946, 2001.
- Mayer, D. A., R. L. Molinari, and J. F. Festa, The mean and annual cycle of upper layer temperature fields in relation to Sverdrup dynamics within the gyres of the Atlantic Ocean, *J. Geophys. Res.*, **103**, 18545-18,566, 1998.
- Mayer, D. A., and R. H. Weisberg, A description of COADS surface meteorological fields and the implied Sverdrup transports for the Atlantic Ocean from 30° S to 60° N, *J. Phys. Oceanogr.*, **23**, 2201-2221, 1993.
- Meinen, C. S., Structure of the North Atlantic current in stream-coordinates and the circulation in the Newfoundland basin. *Deep Sea Res.*, **48**, 1553-1580, 2001.
- Merle, J., and S. Arnault, Seasonal variability of the surface dynamic topography in the tropical Atlantic Ocean, *J. Mar. Res.*, **43**, 267-288, 1985.
- Molinari, R. L., D. A. Mayer, J. F. Festa, and H. Bezdek, Multi-year variability in the near surface temperature structure of the midlatitude western North Atlantic Ocean. *J. Geophys. Res.*, **102**, (C2), 3267-3278, 1997.
- Richardson, P. L., and W. J. Schmitz Jr., Deep cross-equatorial flow in the Atlantic measured with SOFAR floats, *J. Geophys. Res.*, **98** 8371-8387, 1993.
- Roemmich, D., Sea level change, Geophysics Study Committee, Commission on Physical Sciences, Mathematics, and Resources, National Research Council. Sea level and the thermal variability of the ocean, Chapter 13, National Academy Press, Wash., D.C., 208-217, 1990.
- Rosby, T., and R. L. Benway, Slow variations in mean path of the Gulf Stream east of Cape Hatteras, *Geophys. Res. Lett.*, **27**, 117-120, 2000.
- Sciremammano, F. Jr., A suggestion for the presentation of correlations and their significance levels. *J. Phys. Oceanogr.*, **9**, 1273-1276, 1979.
- Stammer, D., Steric and wind-induced changes in TOPEX/POSEIDON large scale sea surface topography observations, *J. Geophys. Res.*, **102**, 20987-21009, 1997.

- Stammer, D., and C. Wunsch, De-aliasing of global high frequency barotropic motions in altimeter observations, *Geophys. Res. Lett.*, **27**, 1175-1178, 2000.
- Talley, L. D., and M. E. Raymer, Eighteen degree water variability, *J. Mar. Res.*, **40** (Suppl.), 757-775, 1982.
- Warren, B., Approximating the energy transport across oceanic sections, *J. Geophys. Res.*, **104**, 7915-7919, 1999.
- Weingartner, T. J., and R.H. Weisberg, A description of the annual cycle in sea surface temperature and upper ocean heat in the equatorial Atlantic, *J. Phys. Oceanogr.*, **21**, 83-96, 1991.